IChemE
www.ingentaselect.com/titles/02638762.htm

0263–8762/04/$30.00+0.00

Trans IChemE, Part A, June 2004
Chemical Engineering Research and Design, 82(A6): 737–751

SIMULATION OF FLOW GENERATED BY AN AXIAL-FLOW IMPELLER
Batch and Continuous Operation

A. R. KHOPKAR[1], P. MAVROS[2], V. V. RANADE[1,*] and J. BERTRAND[3]

[1]*Industrial Flow Modeling Group, National Chemical Laboratory, Pune, India*
[2]*Department of Chemistry, Aristotle University, Thessaloniki, Greece*
[3]*Laboratoire de Génie Chimique, UMR CNRS 5503-ENSIACET, Toulouse, France*

It is important to extend and to validate computational flow models to simulate continuous operation of stirred vessels and to capture possible interaction of feed inlet/outlet with the flow generated by impellers. In the present work, we have developed and used a computational model to understand the flow generated by an axial flow impeller in a batch and a continuously operated baffled vessel. A multiple reference frames approach was used to simulate flow generated by the Mixel TT impeller in stirred vessel. The predicted velocity results show reasonably good agreement (qualitative as well as quantitative) with the experimental data. Characteristics of flow around blades of Mixel TT were studied using the computational model. The computational model was extended to simulate flow and mixing in a continuous operation. Simulations were carried out to understand the interaction of the jet emanating from the feed pipe and the flow generated by the impeller. Model predictions were compared with published experimental data, obtained by laser Doppler velocimetry. The differences and similarities between batch and continuous operation are highlighted. Mixing simulations were carried out to examine possible short-circuiting and non-ideal behaviour of the continuous operation of the stirred vessel. Influence of the impeller speed, feed rate and location of inlet/outlet on mixing and on the extent of non-ideality of flow was studied. The computational model and results discussed in this work will be useful for understanding the mixing process in continuous-flow stirred vessels.

Keywords: CFD; stirred vessel; continuous operation; mixing; Mixel TT.

INTRODUCTION

Stirred reactors are commonly used in chemical, mineral processing, wastewater treating and various other industries. They offer maximum flexibility in operation and can be operated in batch as well as in continuous mode. Despite the widespread use of the stirred reactors, the fluid dynamics of stirred reactors is extremely complex and not quite adequately understood yet. In a baffled stirred reactor, the flow around the rotating impeller blades interacts with the stationary baffles and generates a complex three-dimensional, re-circulating turbulent flow. Obviously, the shape and size of the impeller has a profound influence on the generated flow characteristics. Impellers with several different shapes are used in practice, and new shapes of impeller blades are continuously proposed to achieve better flow characteristics.

Mixel (impeller manufacturing company in France) introduced a hydrofoil-type three-blade axial-flow impeller, called 'TT'. The Mixel TT impeller was found to have better flow characteristics in terms of power and flow number, than the widely used pitched-blade turbines (Aubin *et al.*, 2001; Mavros *et al.*, 2002). *Baudou et al.* (1997) and Mavros *et al.* (1996, 2000) have experimentally studied flow generated by this impeller in a stirred vessel for single as well as for multiple impeller configurations, using laser Doppler velocimetry (LDV). It was, however, not possible to measure the details of flow around the blades of the Mixel TT. Experimental studies also have limitations regarding the range of parameters that can be studied. A computational fluid dynamics based model was therefore developed in this work to simulate the flow generated by the Mixel TT impeller. A multiple reference frames (MRF) approach was used to simulate the flow in the stirred vessel. This approach does not require any experimental data to specify impeller boundary conditions. A commercial CFD code Fluent 5.3 (of Fluent Inc., USA) was used to carry out the flow simulations. The blades of the Mixel TT have four sections with different angles. The characteristics of flow around these blades of complex shapes were studied using the computational model.

*Correspondence to: Dr V. V. Ranade, Industrial Flow Modeling Group, National Chemical Laboratory, Pune 411008, India.
E-mail: vvranade@ifmg.ncl.res.in

Stirred vessels are routinely used as continuous reactors in process industries. Mavros *et al.* (1997, 2000) measured liquid velocities with a LDV apparatus in a continuous-flow stirred vessel, equipped with the Mixel TT impeller in a standard-configuration cylindrical vessel. However, it is not always possible or convenient to determine the fine details of the flow by LDV, especially in continuous-flow systems. It is very expensive and time-consuming to investigate experimentally every possible combination of parameter values and its effect on the vessel/reactor performance. A computational-fluid-dynamics (CFD) based model was therefore extended to simulate the flow generated by the Mixel TT in a continuous-flow stirred vessel. The experimental geometry used by Mavros *et al.* (2000) was considered for these simulations. Mavros *et al.* (2000) carried out experiments with two different ratios of residence time to mixing time and inlet pipe location, in order to examine their effect on the flow behaviour in stirred vessel. In the present work, the computational model was used to understand the interaction of the jet emanating from the feed pipe and the impeller-generated flow. The influence of the impeller speed, feed rate and location of inlet/outlet on mixing and on the extent of non-ideality of flow was studied. The computational model and the predicted results discussed in this work will be useful for understanding flow characteristics in a continuous stirred vessel.

MATHEMATICAL MODELING

The interaction of the rotating impeller blades and of the stationary baffles generates an inherently unsteady flow. Recently, Ranade (2002) has reviewed the various approaches for simulating flow in a stirred vessel. Following his recommendations, quasi-steady state approaches like the 'multiple reference frame' approach or the 'computational snapshot' approach may be adequate for the purpose of the present study. In this work, the MRF approach was selected for simulating the flow generated by the Mixel TT.

In this approach, the whole vessel was divided into two regions: an inner region attached to the rotating impeller and shaft and an outer region attached to the stationary baffles and the vessel. The model equations for the inner region were solved using a rotating framework, whereas the equations for the outer region were solved using a stationary framework. The solution was matched at the interface between the rotating and stationary region via velocity transformation from one frame to the other. This velocity-matching step implicitly involved the assumption of steady flow conditions at the interface. Two approaches were available for modelling the communication between two regions (Marshall *et al.*, 1996). In the first approach, flow characteristics are circumferentially averaged at the interface and then used as boundary condition for the other region. In the second approach, no averaging is carried out and the continuity of absolute velocity is forced to provide the neighbouring values of velocity for the region under consideration. In the present work second approach was used for communicating the two regions (see Fluent manuals for the governing equations). While implementing the MRF approach, several issues such as the extent and position of the inner region, the number of computational cells, the discretization schemes, the turbulence model, the specific position of impeller blades and so on need appropriate selection. The basis for this is discussed below.

In the present work, the experimental set-up used by Mavros *et al.* (2000) was considered. All the relevant dimensions like the impeller diameter, the vessel shape and diameter and so on were the same as those used by Mavros *et al.* (2000). The system investigated consists of a stirred cylindrical reactor, with a dished bottom (diameter, $T =$ height, $H = 0.19\,\text{m}$, $R = 0.19\,\text{m}$) with four baffles (width $= T/10 = 0.019\,\text{m}$) equally spaced around the vessel periphery. The shaft (diameter $d_s = 0.008\,\text{m}$) of the impeller was concentric with the reactor axis and extended to the bottom of the reactor.

An axial flow Mixel TT impeller (diameter, $D = 0.095\,\text{m}$) was used for all simulations. The impeller off-bottom clearance was 0.095 m (measured from the agitator mid-plane). For the continuous-flow mode, the inlet pipe (diameter $d_{in} = 0.01\,\text{m}$) was located above the impeller, with its tip 0.048 m below the liquid surface and 0.011 m away from the shaft. The liquid outlet (diameter, $d_{out} = 0.05\,\text{m}$) was located at the center of the bottom of the reactor. Considering the geometry and the intended extension to a continuous-flow system, the whole vessel was considered as the solution domain. Location of the boundary between inner and outer regions may have some influence on predicted results (Ranade and Tayalia, 2000; Ranade *et al.*, 2001). To minimize such influence, in the present work, the boundary of the inner region was positioned at $r = 0.064\,\text{m}$ (exactly in between the impeller blade tip and baffle) and $0.04\,\text{m} \le z \le 0.13\,\text{m}$ (where z is axial distance from the bottom of the vessel). The solution domain and the inner region considered in the simulations are shown in Figure 1(a).

A commercial grid-generation tool, GAMBIT 1.3 (of Fluent Inc., USA) was used to model the geometry and to generate the body-fitted grids. It is very important to use an adequate number of computational cells while numerically solving the governing equations over the solution domain. The prediction of turbulence quantities is especially sensitive to the number of grid nodes and grid distribution within the solution domain. Our previous work (Ranade *et al.*, 2002) as well as other published work (e.g., Ng *et al.*, 1998; Wechsler *et al.*, 1999) gives adequate information to understand the influence of the grids on the predicted results. It was demonstrated that, in order to capture the trailing vortices accurately, it is necessary to use at least 200 grid nodes to resolve the blade surface. Based on previous experience and some preliminary numerical experiments, about 283,500 computational cells were used for the simulations of the batch and continuous operations. The solution domain and the typical grid used are shown in Figure 1. In the present work, we used the QUICK (Quadratic Upstream Interpolation for Convective Kinetics) discretization scheme with limiter function (SUPERBEE of Roe, 1985) to avoid non-physical oscillations. The results (discussed in the following section) seem to indicate that the number of grid nodes used is sufficient to capture most of the important features of the flow generated by the Mixel TT impeller.

An appropriate turbulence model needs to be selected to simulate the turbulent flow generated in the baffled stirred vessel. Most of the other researchers in this field have used the standard k–ε model (Ng *et al.*, 1998; Brucato *et al.*, 1998; Wechsler *et al.*, 1999). Moreover, recent studies (see

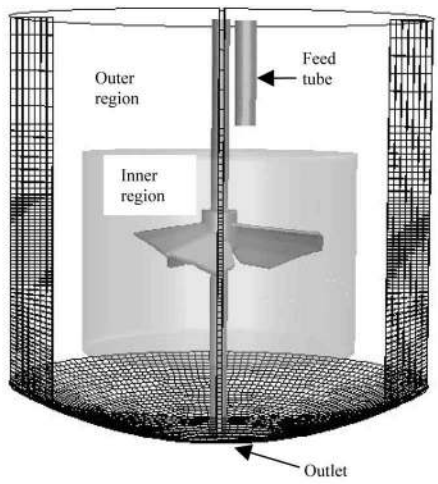

(a) Solution Domain

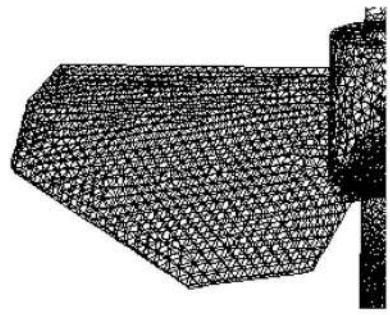

(b) Grid Distribution on Impeller Blade

Grid Details :	
r × θ × z	: 60 × 75 × 63
Total Grid	: 283,500 Cells
Inner Region	: 0.05 m < z < 0.13 m
	r < 0.072 m
	140,844 Cells
Outer Region	: 142,656 Cells

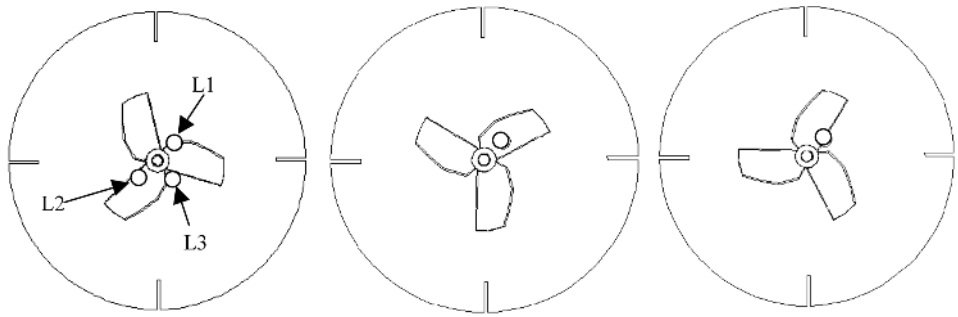

Position 1 (L1 configuration) Position 2 Position 3

(c) Three Specific Positions of Impeller Blades, Feed tube and Baffles

Figure 1. Solution domain and computational grid. (a) Solution domain; (b) computational grid; (c) three specific positions of impeller blades and feed-tube. This figure can be found in colour at www.ingentaselect.com/titles/02638762.htm

for example, Jenne and Reuss, 1999) have indicated that different time scales and anisotropy considerations are of minor importance and do not lead to significant improvements over the standard k–ε model. More often than not, the number of nodes and the quality of the computational grid influence the predicted results more than the underlying turbulence model. Therefore, in the present work the standard k–ε model was used to model the prevailing turbulence.

Wall functions were used to specify wall boundary conditions. The top surface of the liquid pool was assumed to be flat and was modeled as symmetry (zero normal velocity and zero shear). For the continuous-flow mode, the face of the inlet pipe was defined as the inlet. The uniform inlet liquid velocity (corresponding to a liquid flow rate, $Q_l = 2.01667 \times 10^{-4}\,m^3\,s^{-1}$) was specified. Turbulence at the inlet was set by specifying turbulence intensity (10%) and turbulent length scale ($l = 0.07 * R_{in}$, where R_{in} is the hydraulic radius of the feed tube). The outlet of the reactor was modeled as zero gradient boundary condition. The gradients normal to the outlet boundary were set to zero for all the variables except pressure. If the direction normal to the outlet boundary is denoted by y, the outlet boundary condition can be expressed as:

$$\frac{\partial \phi}{\partial y} = 0 \tag{1}$$

It should be noted that, in quasi-steady-state approaches, like MRF or the computational snapshot approach, a specific position of the impeller blades with respect to other stationary internals is considered. In most experimental studies, flow measurements are carried out in a fixed position for several rotations of the impeller. Thus, the measured flow characteristics are essentially averaged over different relative impeller blade positions. In order to make meaningful comparisons, it would be necessary to carry out simulations at different blade positions and then use ensemble-averaged results over these different simulations for comparison. Our previous work has shown that, for batch vessels with geometrically simple impellers like Rushton turbine, there is not much difference between angle-averaged profiles and ensemble averaged profiles (see for example, Ranade and van den Akker, 1994). In the present case, however, it was observed that the complicated shape of the impeller and interaction of inlet jet with the impeller stream leads to some differences in ensemble averaged results and angle-averaged results. We therefore carried out simulations at three different relative positions of impeller blade with respect to baffles and inlet/outlet. It may be noted that one simulation provides data at four mid-baffle planes for a specific position of impeller blades with respect to baffles and inlet/outlet. The results from three simulations were used to obtain ensemble-averaged profiles at mid-baffle plane (based on a total of 12 planes). For batch operations the predicted results were ensemble averaged over all 12 mid-baffle planes and then compared with the experimental data. For continuous-flow operation, a number of different relative blade positions with respect to the feed inlet and baffles respectively are possible. Initially, different relative blade positions with respect to the feed inlet were considered to understand the interaction of incoming feed with the impeller. In these three cases, the specific position of impeller blades with respect to baffles was kept the same. Then three different relative positions of impeller blades with respect to baffles were considered and the predicted results were ensemble averaged for comparison with the experimental data. In all the cases, the feed inlet was located at the mid-baffle plane as in the experiments. The five configurations considered in this work are shown in Figure 1(c). These five configurations can adequately represent the flow in a continuous-flow stirred reactor.

A commercial CFD code, Fluent 5.3 (of Fluent Inc., USA) was used to carry out flow simulations. The fluid properties were set as: viscosity of liquid (μ) = 0.0009 Pa s and density of liquid (ρ) = 1000.0 kg m^{-3}. For initiating computations, all variables except k and ε were set to zero. The initial values of k and ε were set to 0.0001 with appropriate units. The converged results were not found to be affected by the initial conditions. Computations were carried out for two impeller rotational speeds (180 and 360 rpm) and one liquid inlet flow rate ($Q_1 = 2.01667 \times 10^{-4}$ m^3 s^{-1}). All computations were carried out until the normalized residues fell below 0.0001.

Converged flow results were used for further simulations of mixing in the stirred vessel. For simulating mixing in a continuous-flow operation, a square pulse of tracer was introduced in the inlet stream for 1 s. The evolution of the tracer concentration field within the vessel and its outlet concentration with respect to time were simulated and studied. The time step used for all the mixing simulations was 0.01 s. The species transport equations were solved for adequate time to ensure the complete removal of tracer material from reactor (more than four times the mean residence time, $\tau = 25.23$ s). The simulated tracer concentration fields and the residence time distributions were analysed to examine possible non-ideal flow behaviour. The computational results are discussed in the following section.

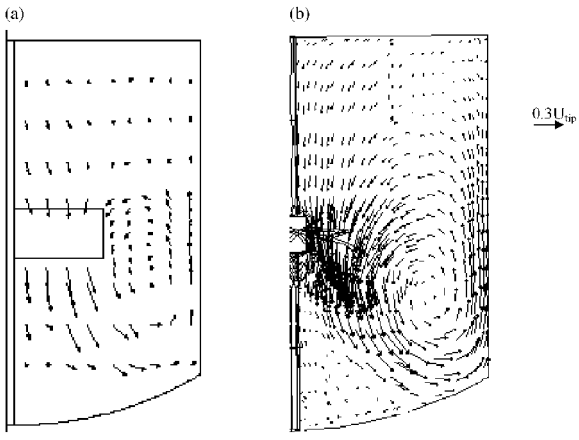

Figure 2. Mean flow field at r–z plane for batch operation, $N = 360$ rpm and $U_{tip} = 1.7907$ m s^{-1}. (a) Experimental—mid-baffle plane (Mavros *et al.*, 2000); (b) predicted—mid-baffle plane.

RESULTS AND DISCUSSION

Batch Operation: Global Flow Characteristics

The flow generated by the Mixel TT impeller in a batch vessel was simulated for an impeller rotation speed of 360 rpm. Without using any impeller boundary conditions, the MRF approach was able to simulate the axial flow pattern generated by the impeller. The comparison of the predicted velocity field (ensemble averaged to eliminate the influence of specific blade position) and experimental LDV data (mid-baffle position) is shown in Figure 2. A high velocity jet emanating from the bottom of the impeller and a small reverse loop below the hub, seen in the experimental flow field, are also captured in the simulations.

Quantitative comparison of the predicted results and the experimental data of Mavros *et al.* (2000) is shown in Figure 3. It can be seen from Figure 3(a) that the comparison between the predicted values of axial velocity and experimental data was satisfactory. The maximum axial velocity in the downward direction, at a height of 0.07 m from the bottom of the vessel, was about 0.45 times the impeller tip velocity (not shown in Figure 3a). The measured and predicted axial velocity field was used for calculating the flow (or pumping) number for the Mixel TT as:

$$N_Q = \frac{2\int \pi r U \, dr}{ND^3} \tag{2}$$

The limits of integration for the radial distance are from the surface of the shaft to the impeller radius. The predicted pumping number for Mixel TT (0.612) is in good agreement

with the reported experimental value of 0.67 (Aubin *et al.*, 2001).

It can be seen (Figure 3b) that the comparison of the predicted and experimental radial mean velocities was also reasonably good. For a small region above the impeller, the predicted radial profiles showed some deviation from the experimental data. The magnitude of such deviation was small. Agreement between predicted and experimental data for the tangential mean velocity was also reasonably good as that for the axial velocity. Tangential velocity profiles at the mid-baffle plane showed some reverse circulation above the impeller, which was captured in the simulations (see Figure 3c).

The values of the turbulent kinetic energy were rather over-predicted (Figure 3d), especially in the region below the impeller. Reasons for these observed discrepancies are not obvious. The use of more complex models, like the Reynolds stress models, is not an answer to this problem, since it does not lead to any significant improvement over the standard k–ε model (see Jenne and Reuss, 1999). The observed discrepancies, however, may not be a serious impediment to many reactor-engineering applications since some chemical engineering applications like blending are not sensitive to the turbulence levels and are controlled by mean flow. For example, Ranade *et al.* (1991) has demonstrated that predicted mixing time in stirred vessels is not significantly affected by turbulent dispersion (order of magnitude change in the turbulent dispersion coefficient resulted in change of few percent in predicted mixing time). Correct prediction of turbulence levels is important for applications controlled by turbulence quantities like dispersion of bubbles or micromixing. Fortunately, even in many such applications, the relevant processes depend on fractional power of turbulence energy dissipation rate (for example, prediction of Sauter mean diameter depends on $\varepsilon^{0.4}$). Thus 30% over-prediction of energy dissipation rates leads to smaller (14%) error in Sauter mean diameter. Therefore, in the present work, we extended this computational model to understand the mixing process in a continuous-flow stirred vessel equipped with this (Mixel TT) impeller. However, before we discuss simulations of the continuous-flow operation, it would be useful to examine the flow characteristics near the blades of the Mixel TT impeller, in order to understand the role of their special blade shape.

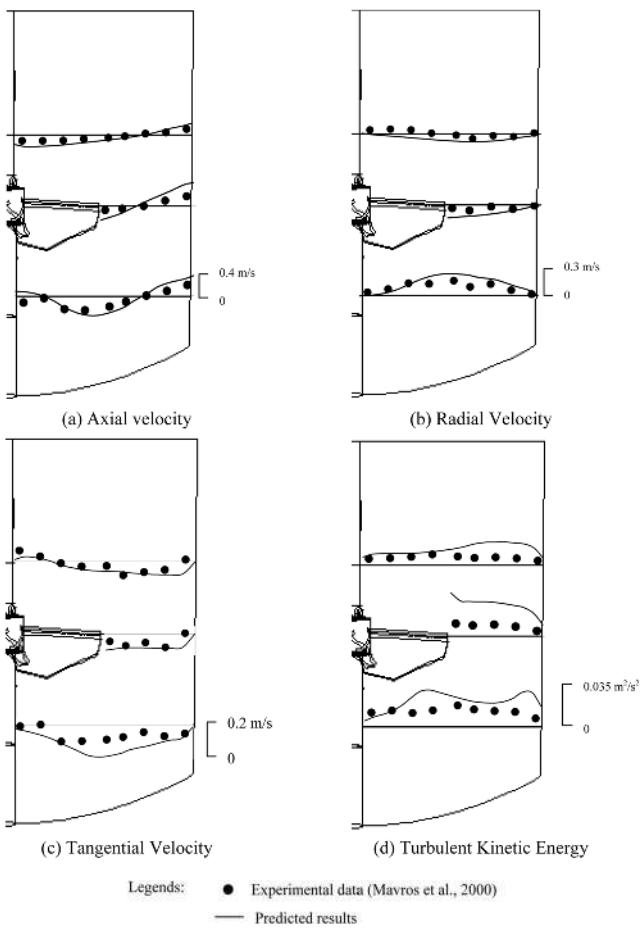

Figure 3. Comparison of predicted results and experimental data for batch operation, $N = 360\,\text{rpm}$ and $U_{\text{tip}} = 1.7907\,\text{m s}^{-1}$.

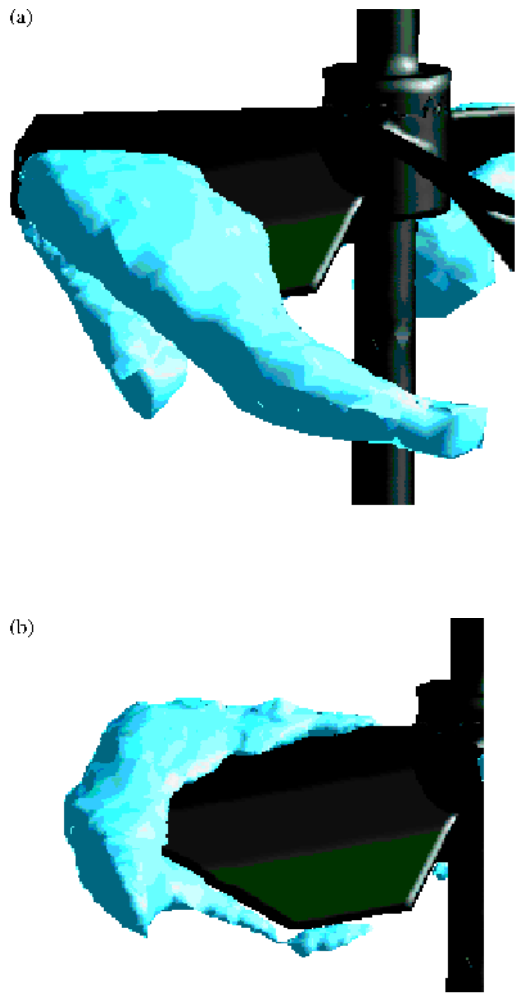

Figure 4. Flow field around impeller blades for batch operation, $N = 360\,\text{rpm}$ and $U_{\text{tip}} = 1.7907\,\text{m s}^{-1}$. (a) Iso-surface of axial velocity jet (iso-value $= 0.6\,\text{m s}^{-1}$ in downward direction); (b) iso-surface of turbulent kinetic energy (iso-value $= 0.06\,\text{m}^2\text{s}^{-2}$). Impeller is moving inwards through the paper. This figure can be found in colour at www.ingentaselect.com/titles/02638762.htm

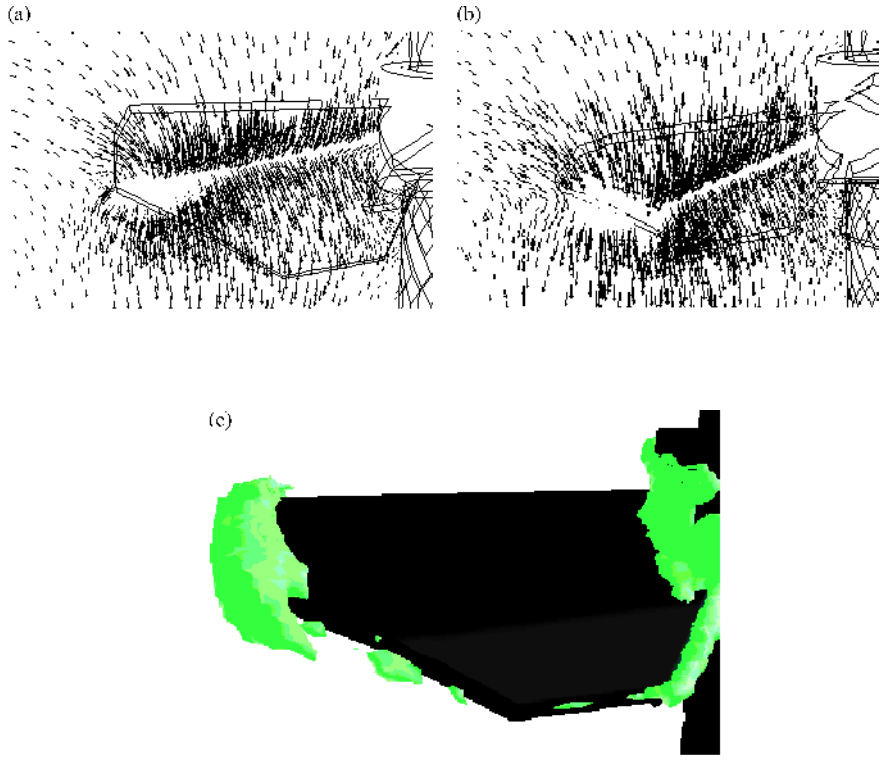

Figure 5. Flow field around impeller blades for batch operation, $N = 360\,\text{rpm}$ and $U_{\text{tip}} = 1.7907\,\text{m s}^{-1}$. (a) $\theta = 20°$ behind leading edge of impeller blade; (b) $\theta = 37.5°$ behind leading edge of impeller blade; (c) iso-surface of Z-vorticity, $\omega = 75\,\text{s}^{-1}$. Impeller is moving inwards through the paper. This figure can be found in colour at www.ingentaselect.com/titles/02638762.htm

Flow Around Blades of Mixel TT Impeller

Similar to the down-flow pitched-blade turbine, the Mixel TT impeller generates high velocity jets moving downwards. An iso-surface of axial velocity around an impeller blade is shown in Figure 4(a). It can be seen that the jet emanating from the front side is faster than that emanating from the back of the blade. The jet flowing downwards from the back of the blade appears to interact with the trailing vortex attached to the back of the blade.

An iso-surface of turbulent kinetic energy is shown in Figure 4(b). The leading edge of the blade generates the highest turbulence. The movement of the blade generates a high-pressure region ahead of the blade leading edge, and a low-pressure region behind the blade. Such a pressure difference leads to a trailing vortex behind impeller blades. Prediction of pressure field around impeller blades and of trailing vortex is especially crucial for extending the present approach for simulations of multiphase flows generated by impellers. The examination of the predicted results indicates that the pressure field seems to be simulated correctly.

In order to examine the trailing vortex, a close-up of the velocity field behind the impeller blade was examined. Vector plots at r–z planes located at two different angles behind the impeller blade are shown in Figure 5(a) and 5(b). These vector plots clearly indicate the presence of a single vortex trailing behind the impeller blade. The center of the vortex appears to move away and downwards from the impeller. The presence of the trailing vortex is more clearly seen from the iso-surface of vorticity shown in Figure 5(c).

The computational model was thus successful in capturing the major features of the flow generated by the Mixel TT impeller in the stirred reactor. The comparison of simulated and reported experimental results shows reasonably good agreement. The model was then extended to simulate continuous operation with Mixel TT impeller.

Continuous Operation

In a continuous-flow stirred reactor, apart from the size, shape, location and rotation speed of the impeller, the fluid dynamics are also a complex function of the inlet and outlet locations and of the liquid flow rate. Such complex fluid dynamics ultimately control whether the behaviour of the continuous-flow reactor is closer to the ideal, single CSTR or far from it. Customarily, the ratio of residence time and mixing time is kept high (>10) to avoid non-ideal flow behaviour in stirred reactors. The residence time (τ) is calculated from the ratio of the reactor volume (V_{l}) and the liquid flow rate (Q_{l}). The value of mixing time (t_{m}) is a function of impeller design and impeller rotational speed.

Mavros *et al.* (2000) studied the fluid dynamics of a continuous-flow stirred vessel equipped with a Mixel TT impeller at two different ratios of residence time and mixing time. In both cases, the liquid flow rate was kept constant and equal to $2.01667 \times 10^{-4}\,\text{m}^3\,\text{s}^{-1}$. Two values of impeller speed were studied, to realize two values of the ratio of residence time to mixing time (predicted from the correlation of Roustan and Pharamond, 1988) as 9.6 and 4.8

(impeller speed of 360 and 180 rpm respectively). At the impeller speed of 360 rpm ($\tau/t_m = 9.6$), the vessel was expected to behave almost like an ideal CSTR. At the lower impeller speed ($\tau/t_m = 4.8$), non-ideal flow (non-ideal mixing) behaviour of the stirred reactor could be a distinct possibility. In this work, we extend our computational model to study these two cases of continuous-flow operation.

Comparison with experimental data: for N = 360 rpm

In a continuous-flow operation, if the feed inlet is located in such a way that the high-velocity incoming jet passes through an opening between the impeller blades, the resulting flow field may be different from the one when the inlet is located in such a way that the high-velocity jet impinges on the blade. Therefore, as discussed above, three specific blade positions with respect to feed inlet were considered. In the

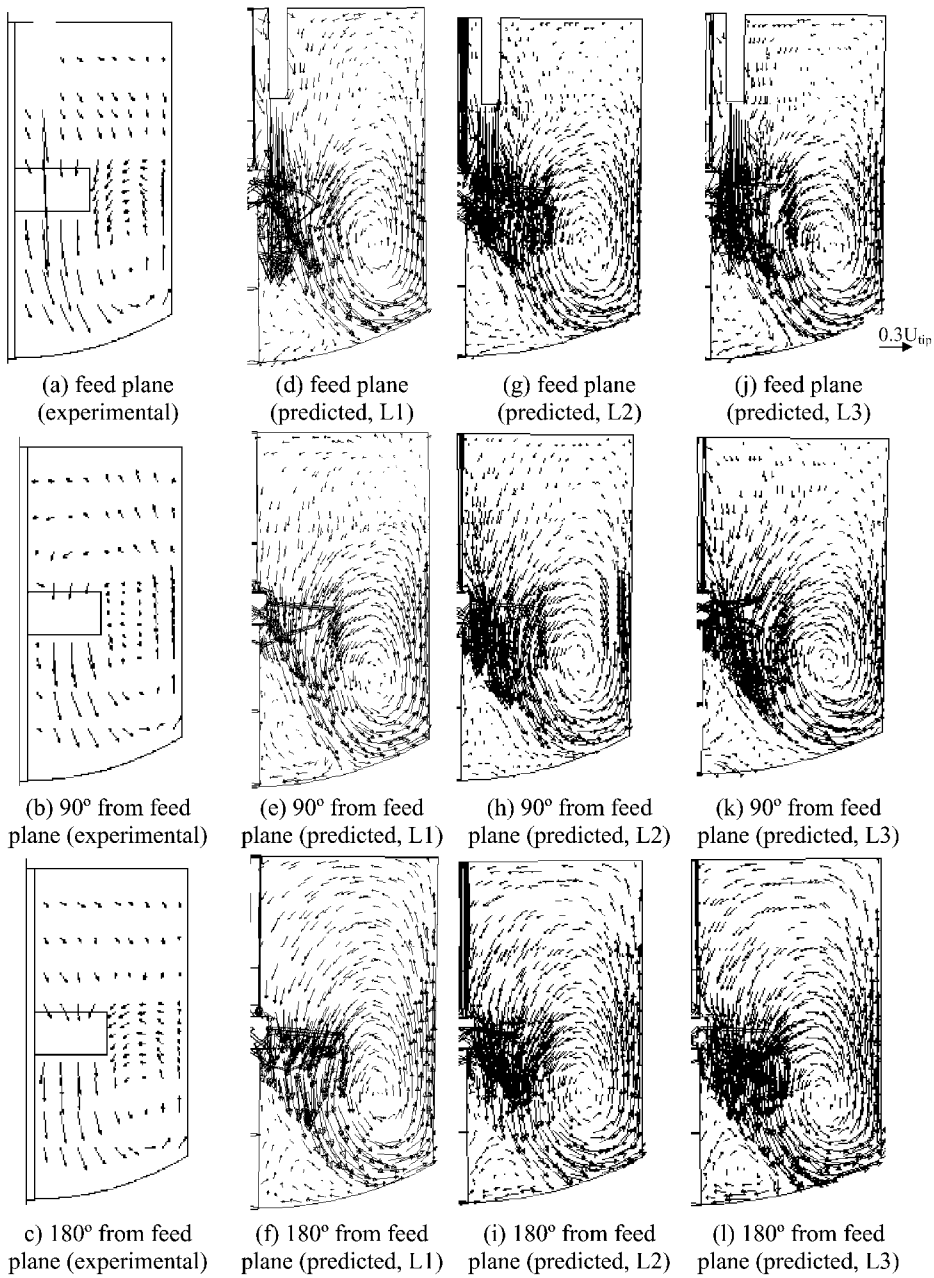

Figure 6. Mean flow field at three r–z planes for continuous operation for three specific positions of impeller blades and feed-tube, $Q_1 = 2.01667 \times 10^{-4}\,m^3 s^{-1}$, $N = 360$ rpm and $U_{tip} = 1.7907\,m\,s^{-1}$.

	Experimental	Predicted
Feed plane	(a)	(d, g, j)
90° from feed plane	(b)	(e, h, k)
180° from feed plane	(c)	(f, i, l)

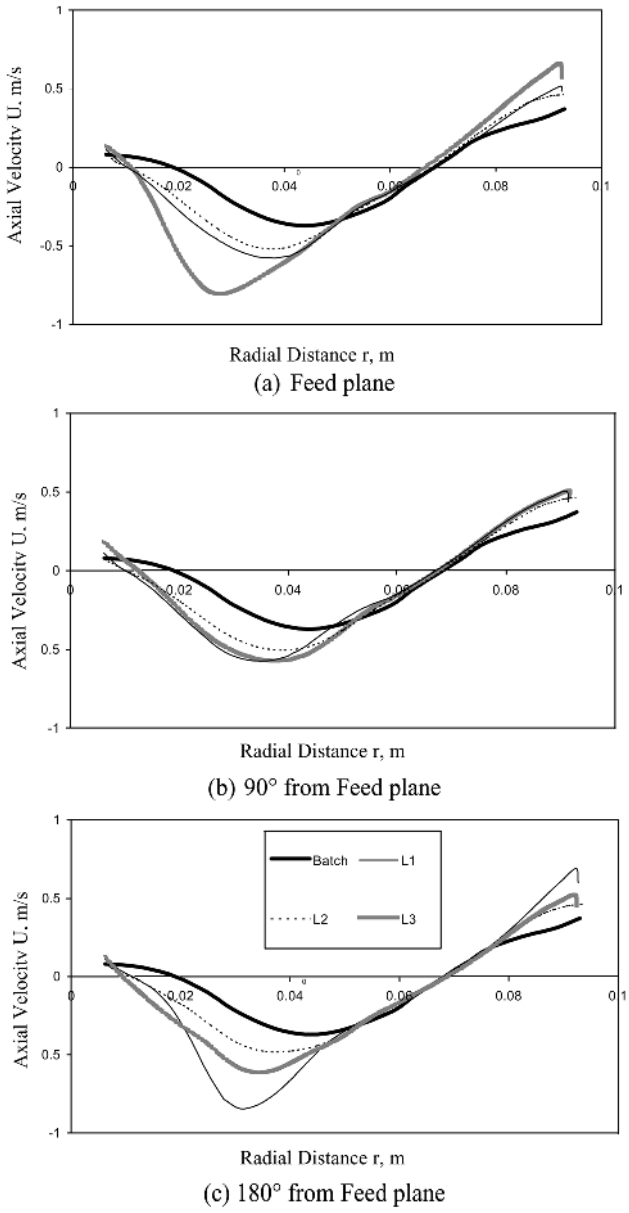

Figure 7. Comparison of axial velocity for batch and continuous operation (for three specific positions of impeller blades and feed-tube), $Q_1 = 2.01667 \times 10^{-4}\,m^3\,s^{-1}$, $N = 360\,rpm$, $U_{tip} = 1.7907\,m\,s^{-1}$ and $z = 0.05\,m$.

first configuration, the feed tube was located above the last two sections of an impeller blade. In the second configuration, the feed tube was located above the first two sections of the impeller blade, whereas in the third configuration, the incoming feed was allowed to bypass the impeller through the clearance between two adjacent blades. The feed tube was located at a mid-baffle plane in all configurations considered. Comparisons of the predicted velocity field and experimental data (at three different r–z planes: feed plane, 90° from feed plane and 180° from feed plane) for three configurations are shown in Figure 6.

The simulations captured the high-velocity jets emanating from the feed pipe and the impeller blades and the small reverse loop below the impeller. The location of the circulation 'eye' is lowered and found to be closer to the bottom of the vessel compared with the batch operation. This is in agreement with the experimental observation of Mavros *et al.* (2000). The predicted flow field shows some variations within these three configurations, especially in the region below the impeller. For a quantitative examination of these differences, the predicted values of axial velocity for these three configurations at an axial location of 0.05 m from the vessel bottom were compared with the ensemble averaged results predicted for the batch vessel in Figure 7. It can be seen that there is a significant interaction between the impeller stream and the feed jet. As expected, the predicted axial velocity for configuration L3, in which the feed jet is located in the open space between the impeller blades, is highest. The difference between the predicted results for these three configurations decreases as one moves away from the impeller. For detailed quantitative comparison with experimental data, additional simulations were carried out for three different positions of impeller blades relative to baffles and the flow characteristics were ensemble averaged.

The ensemble-averaged results were compared with the experimental data of Mavros *et al.* (2000) at three different axial locations in Figure 8. It can be seen that the comparison between the predicted axial velocity values and the experimental data is reasonably good. Higher values of axial velocities were predicted below the feed pipe and near the vessel wall. The incoming jet combines with the liquid being drawn by the impeller, and hence the axial velocities at the lower side of the impeller are considerably higher than in the batch case. It can be seen that the axial velocities close to the center of the vessel are relatively higher in the plane located at 180° from the feed plane. This indicates that part of the incoming liquid is added to the flow entrained in a tangential motion by the rotating impeller.

The comparison between the predicted radial velocity values and the experimental data is reasonably good. For the feed plane and for the plane at 180° from the feed plane (Figure 8b), experimental data shows outward radial velocity just below the feed pipe. However, the predicted radial velocity profile does not show such outward velocity. For the plane at 180° from the feed plane, radial velocity values at 0.05 m from the bottom are rather over-predicted. The comparison of predicted and experimental tangential velocities is shown in Figure 8(c). It can be seen from Figure 8(c) that the comparison between the predicted results and experimental data is satisfactory.

The values of predicted turbulent kinetic energy are compared with the experimental data (Figure 8d). It can be seen that CFD model over-predicted (Figure 8d) the turbulent kinetic energy, especially in the region below the impeller. The predicted turbulence characteristics in the vessel may be sensitive to the turbulence level at the inlet pipe. To quantify such sensitivity, three simulations were carried out with three different turbulence intensity values at the inlet (0.1, 10 and 20%). The simulated results are shown in Figure 9. It can be seen that the inlet boundary conditions do not significantly influence the prediction of turbulence field in the vessel (within the range considered in the present work). Therefore, for all the subsequent simulations, the turbulence intensity of the incoming fluid was set to 10%.

Comparison with experimental data: for $N = 180\,rpm$

Simulations were also carried out at a lower impeller rotation speed of 180 rpm. This lower impeller speed leads

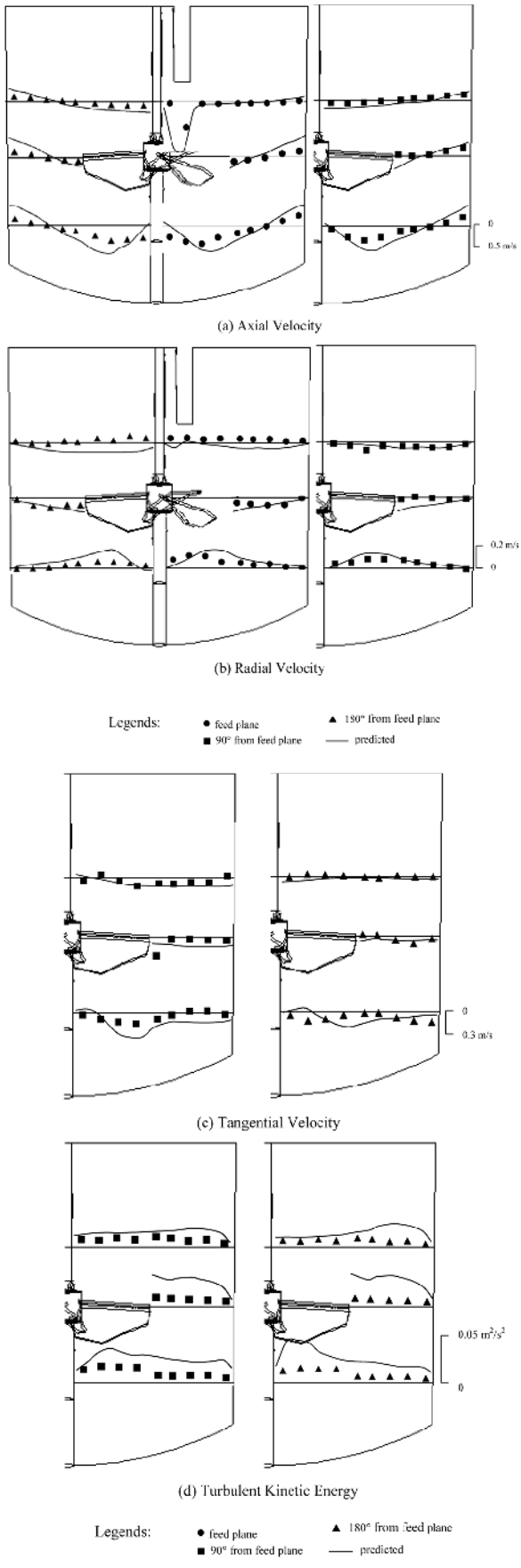

Figure 8. Comparison of predicted results and experimental data for continuous operation, $Q_1 = 2.01667 \times 10^{-4}\,\mathrm{m^3\,s^{-1}}$, $N = 360\,\mathrm{rpm}$ and $U_{tip} = 1.7907\,\mathrm{m\,s^{-1}}$ (symbols denote data of Mavros *et al.*, 2000).

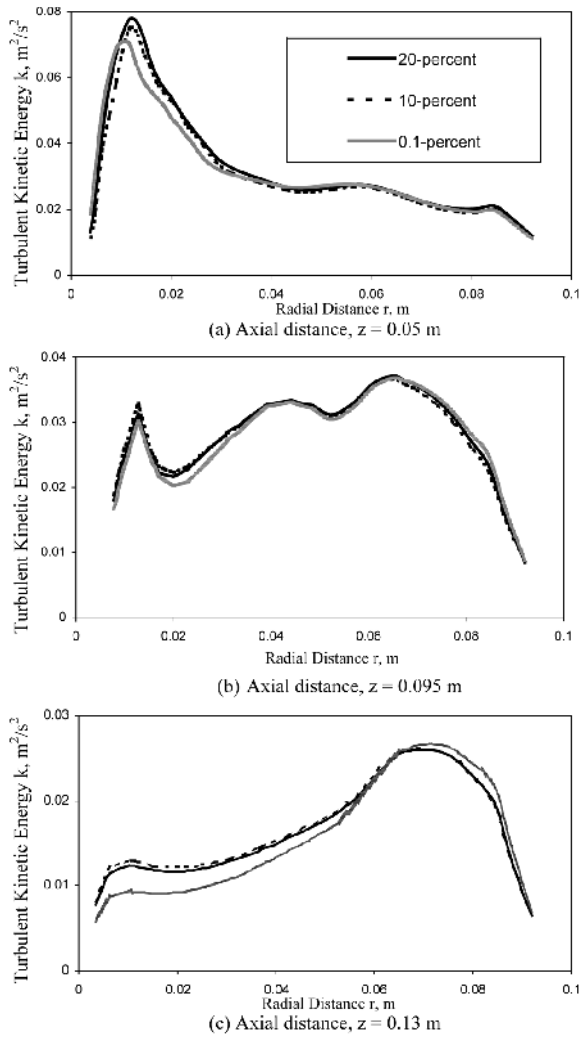

Figure 9. Effect of turbulence intensity at the inlet on the predicted profiles of turbulent kinetic energy, $Q_1 = 2.01667 \times 10^{-4}\,\mathrm{m^3\,s^{-1}}$, $N = 360$ rpm and $U_{tip} = 1.7907\,\mathrm{ms^{-1}}$ [180° from feed plane].

to a decrease in impeller pumping, which will further enhance the influence of the incoming liquid feed on the flow field within the vessel. Comparison of the predicted velocity field and experimental data (at the feed plane, 90° and 180° from the feed plane) is shown in Figure 10. It can be seen from the simulated results that the eye of circulation was moved further towards the vessel bottom, which is in agreement with the experimental observations. The high-velocity feed interacts with the impeller stream and almost no reverse loop is observed for the lower impeller speed.

The quantitative comparison of the predicted results with the experimental data of Mavros *et al.* (2000) at three different axial locations is shown in Figure 11. The comparison between the predicted and experimental axial velocity values is shown in Figure 11(a). The maximum axial velocity was observed below the feed tube (0.13 m from the bottom of the reactor). The axial velocity at the feed inlet was considerably higher than the circulating liquid. The strong incoming jet passes through the impeller region and appears on its lower side. High axial velocities were observed at the bottom of the vessel. This indicates possible short-circuiting.

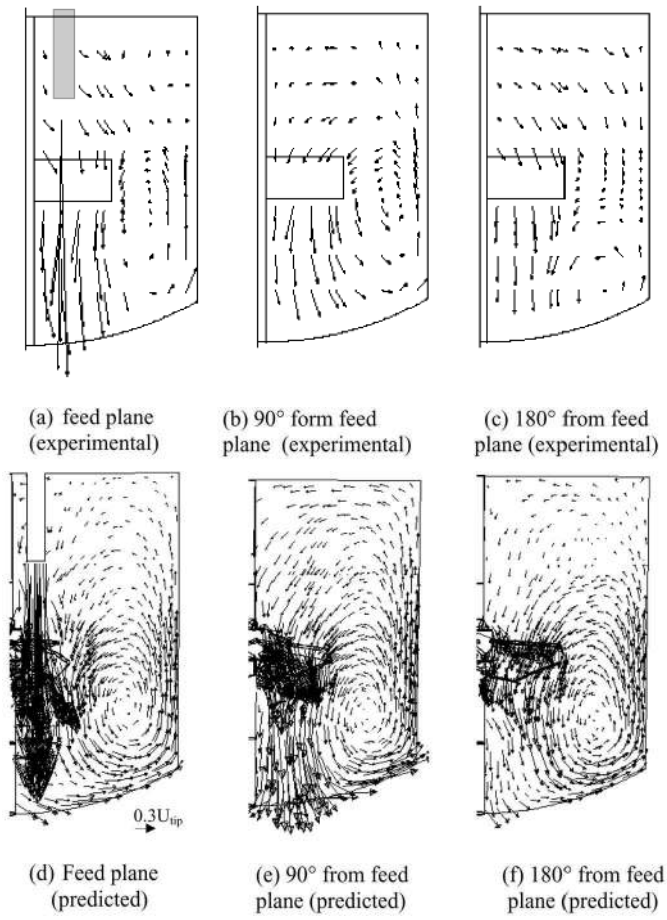

Figure 10. Mean flow field at three r–z planes for continuous operation, $Q_l = 2.01667 \times 10^{-4}\,m^3\,s^{-1}$, $N = 180$ rpm and $U_{tip} = 0.8954\,m\,s^{-1}$.

	Experimental	Simulated
Feed plane	(a)	(d)
90° from feed plane	(b)	(e)
180° from feed plane	(c)	(f)

The comparison of the predicted radial velocity profiles and the experimental data is shown in Figure 11(b). It can be seen that the agreement was reasonably good for the plane at 90° from the feed plane. However, it was not that good for the plane at 180° from the feed plane. For the latter plane, the experimental data shows an outward radial velocity at a 0.05 m height from the bottom of the vessel. The computational model has not captured this. Experimental data of tangential velocities at planes located at 90° and 180° from the feed plane showed very small tangential velocity values, compared with the predictions (Figure 11c). Similar to those predicted for a higher impeller rotational speed, the values of the predicted turbulent kinetic energy were higher than the experimental data (Figure 11d). Although the agreement of the predicted and experimental data for the continuous-flow operation for 180 rpm was not as good as for the batch operation and for the continuous-flow operation for 360 rpm, the simulations seem to capture the key flow characteristics. The computational model was therefore extended to simulate the mixing process and investigate the residence time distribution of the flowing-through liquid.

Mixing in Continuous Stirred Reactor

Mavros *et al.* (2000) studied the fluid dynamics of a continuous-flow stirred vessel equipped with a Mixel TT impeller at two different ratios of residence time and mixing time. In both cases, the liquid flow rate was kept constant and equal to $2.01667 \times 10^{-4}\,m^3\,s^{-1}$. Two values of impeller speed were studied, in order to realize two values of the ratio of residence time to mixing time: 9.6 and 4.8 (at impeller speeds of 360 and 180 rpm, respectively). Usually, continuous operation of a stirred vessel is considered as almost ideal when the ratio of residence time to mixing time is about 10. Considering this, ideal flow behavior would be expected at the higher impeller speed ($\tau/t_m = 9.6$), while a non-ideal behavior would be expected at the lower impeller speed ($\tau/t_m = 4.8$). Computational flow models developed in this work were used to evaluate these expectations.

N = 360 rpm

Simulation of mixing was carried out for an impeller rotation speed of 360 rpm and a liquid flow rate of

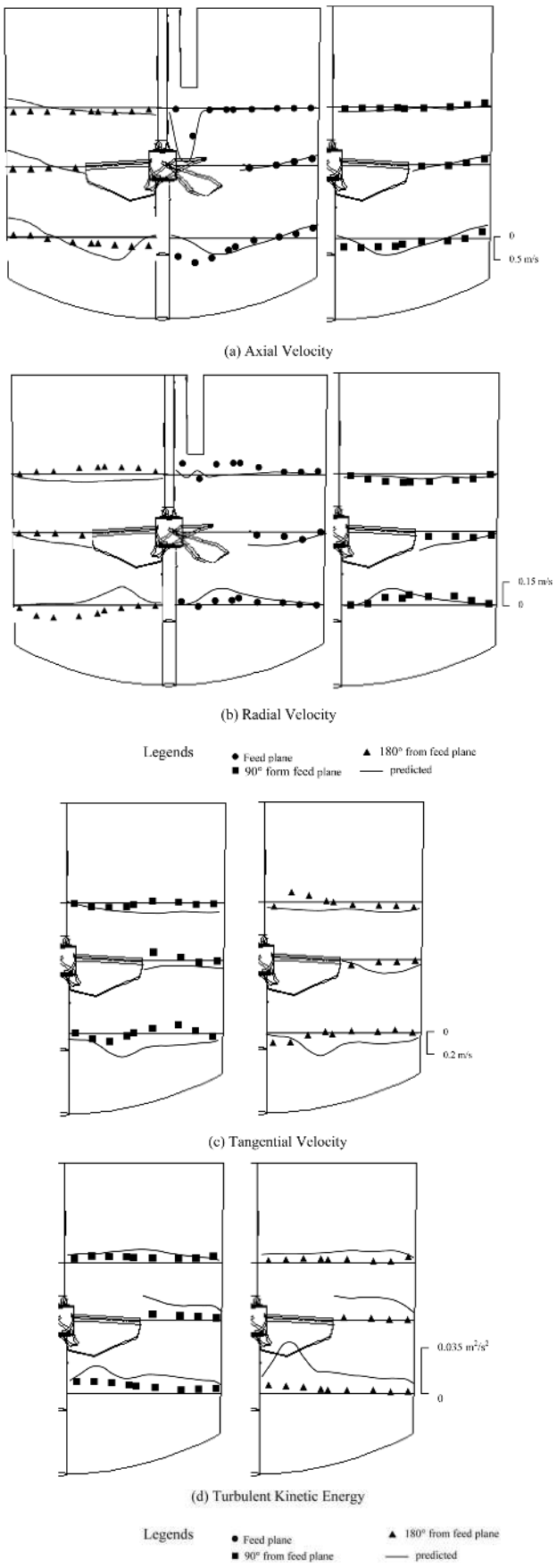

Figure 11. Comparison of predicted results and experimental data for continuous operation, $Q_I = 2.01667 \times 10^{-4}\,m^3\,s^{-1}$, $N = 180\,rpm$ and $U_{tip} = 0.8954\,m\,s^{-1}$ (symbols denote data of Mavros *et al.*, 2000).

$2.01667 \times 10^{-4}\,m^3\,s^{-1}$. Completely converged flow results were used for simulating mixing, assuming that the addition of the tracer does not influence the fluid dynamics in the stirred vessel. An instantaneous square pulse of tracer (at time $t = 0$) was introduced in the reactor through the inlet stream for 1 s (the mass fraction of the tracer at the inlet was set equal to 1). The species transport equations were solved for more than four times of residence time, to ensure the complete removal of tracer material from the reactor.

The evolution of the tracer concentration field within the reactor and the outlet concentration with respect to time was simulated and studied. The predicted snapshots of the tracer concentration field at various times are shown in Figure 12. It can be seen that the tracer follows the liquid circulation path and is pumped downwards by the impeller. It was interesting to note that, even in the case of a high impeller speed, where the ratio of residence time to mixing time is about 10, a significant non-uniformity in tracer concentration existed within the vessel. This indicates a deviation from the ideal CSTR reactor performance and shows a possibility of non-ideal mixing (or non-ideal flow behavior) in the stirred reactor, even for the high ratio of residence time and mixing time.

To examine the non-ideality further, the history of tracer concentration at the outlet of the reactor was studied. Mixing simulations were carried out for all three specific positions of impeller blades and feed tube. The predicted exit age distributions were then compared with that of an ideal CSTR. It can be seen from Figure 13(a) and (b) that the exit age distribution is significantly different from that of the ideal CSTR for all three positions. For the L3 configuration, where the feed tube is positioned above the clearance between two impeller blades, a strong short-circuiting is observed even when the ratio of residence time to mixing time is about 10. The time of first appearance of the tracer at the outlet is about 1 s. From the overshoot in tracer concentration observed at the outlet, it appears that the high velocity inlet jet may be interacting directly with the outlet.

This is further confirmed by the lower slope of predicted residence time distribution curve compared with that of ideal CSTR. The combination of overshoot at the beginning and lower slope at later stage indicates that part of the incoming fluid bypasses stirred vessel and flows effectively through a small volume plug flow reactor and the remaining part of the incoming fluid flows through a stirred vessel with much larger effective residence time than that calculated from the total incoming flow (Figure 13b). The nature of predicted exit age distribution indicates that it can be modeled as a combination of ideal stirred reactor and plug flow reactor operating in parallel. Preliminary analysis indicates that the effective residence time of the ideal CSTR part is about 68 s (this means only about 36% of the incoming liquid flows through a vessel and about 64% of the incoming fluid short circuits to the outlet). To examine the influence of impeller speed, a case of continuous-flow operation at a lower impeller speed was simulated.

$N = 180\,rpm$

The simulated exit age distribution for the lower impeller speed case is also shown in Figure 13 (for configuration L1). The predicted exit age distribution indicates a strong

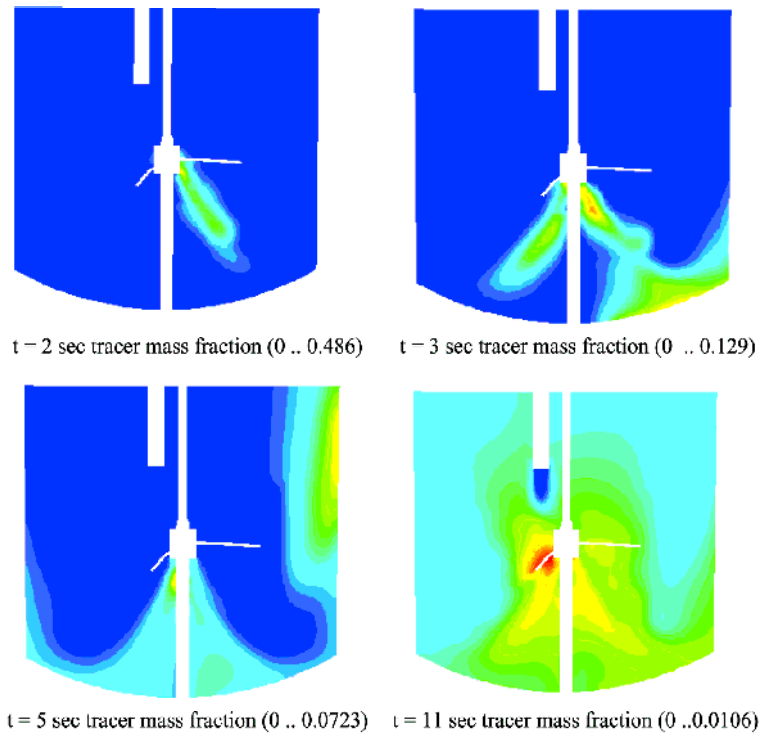

Figure 12. Predicted snapshots of tracer mass fraction at different time, for continuous operation, $Q_l = 2.01667 \times 10^{-4}\,m^3\,s^{-1}$ and $N = 360$ rpm.

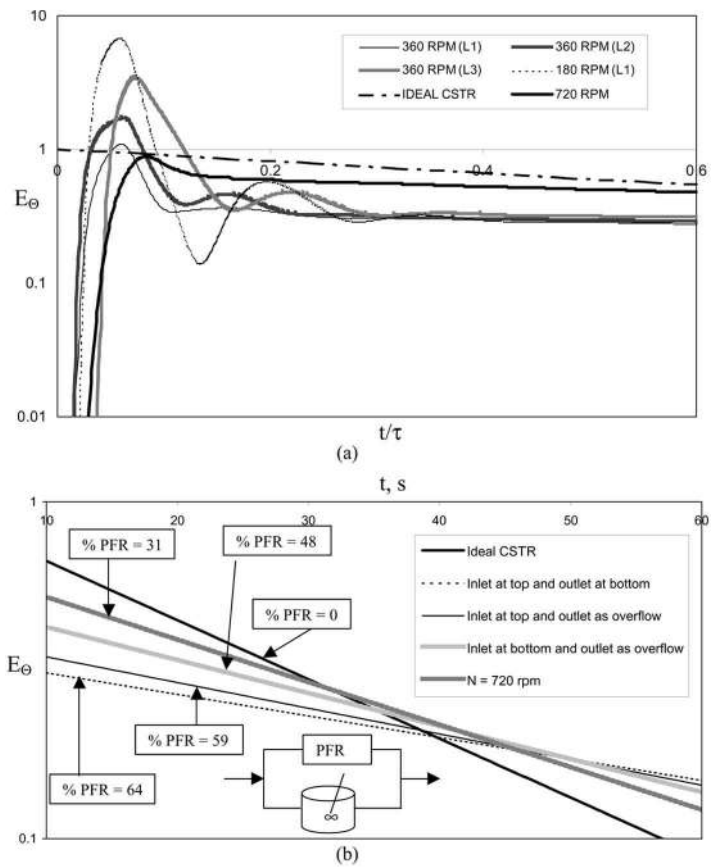

Figure 13. Comparison of predicted exit age distributions with ideal CSTR.

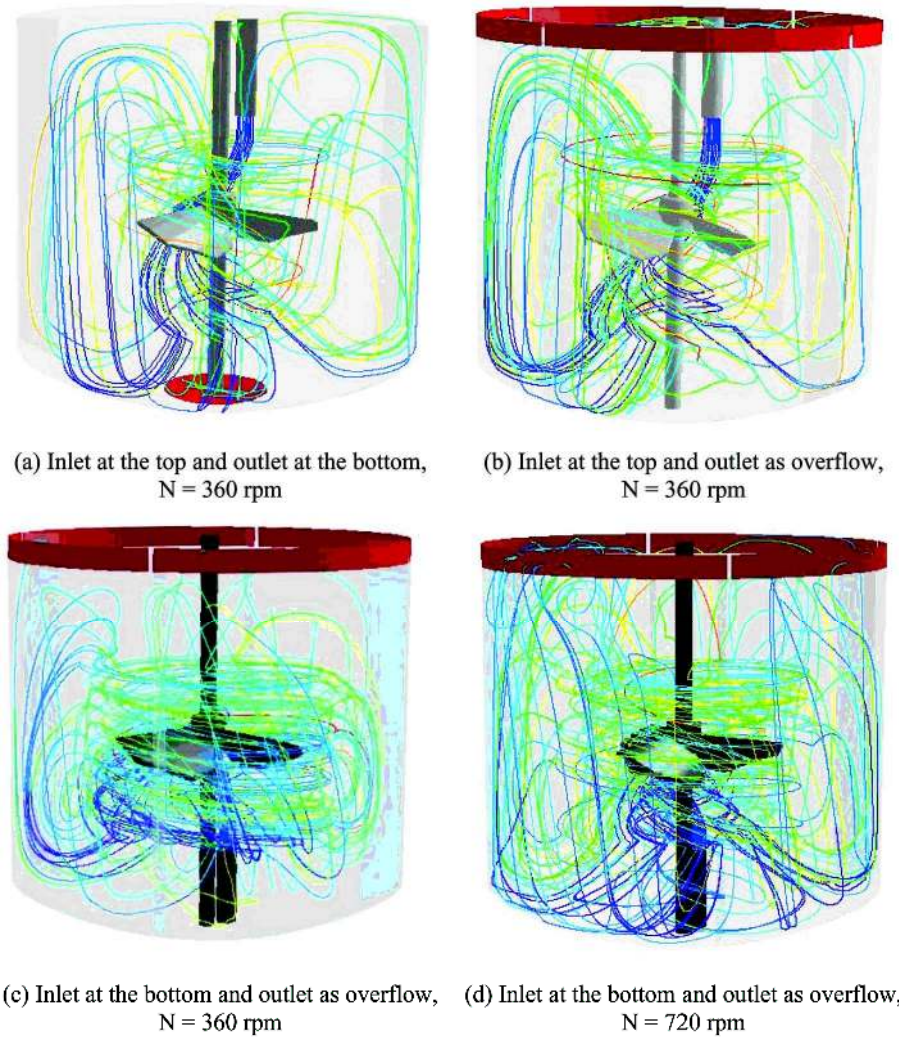

(a) Inlet at the top and outlet at the bottom, N = 360 rpm

(b) Inlet at the top and outlet as overflow, N = 360 rpm

(c) Inlet at the bottom and outlet as overflow, N = 360 rpm

(d) Inlet at the bottom and outlet as overflow, N = 720 rpm

Figure 14. Streak lines for incoming liquid feed for different inlet/outlet configurations, $Q_I = 2.01667 \times 10^{-4}\,m^3 s^{-1}$.

short-circuiting within the stirred reactor. The impeller pumping action is not sufficient to quickly mix the incoming liquid with the circulating liquid. The incoming jet appears to be passing straight through the impeller region towards the outlet. Examination of the simulated velocity vectors (Figure 10) and axial velocity profiles (Figure 11a) at the bottom of the reactor also supports these indications. Analysis of predicted RTD for lower impeller speed using the combination of ideal plug flow and idea CSTR indicates that about 72% of the incoming liquid short circuits to outlet.

Simulations of mixing indicate that, in addition to the relative importance of the impeller rotation speed and feed rate, the locations of the inlet and outlet also have a profound influence on the flow behaviour of continuous-flow stirred reactors. Even if the usual guidelines of keeping ratio of mixing time to residence time more than 5 is followed, incorrect location of inlet and outlet nozzles may lead to severe short-circuiting as observed in the present case. Since the outlet location in the considered geometry was exactly below the impeller, significant part of the tracer short-circuits from the reactor. The early removal of tracer is clearly seen from the snapshots of tracer mass fraction at $t = 3$ and 5 s (Figure 12). A different liquid outlet and inlet configuration would probably improve the performance of the stirred reactor.

Effect of Inlet and Outlet Locations on the Performance of Reactor

To understand the interaction of incoming feed with impeller generated flow particle streak lines were simulated by releasing neutrally buoyant tracer particles from the inlet pipe. The simulated particle streak lines (for a flow time of 5 s) for different configurations are shown in Figure 14. It can be seen from Figure 14a that, when the outlet is located below the feed pipe and impeller speed is not adequate, part of incoming feed stream directly interacts with the outlet and leads to short-circuiting in the reactor. The streaklines show little effect of impeller action on the flow of incoming feed in the reactor. In order to reduce the direct interaction of incoming feed with the outlet location, the position of outlet of reactor was changed. The outlet was modeled as overflow from the vessel. The predicted exit age distribution (Figure 13b) shows some improvement over the case with outlet at the bottom. However, some short-circuiting in the reactor was still found to occur. It can be seen from

Figure 14b that the major fraction of the streak lines is grouped together and does not get homogeneously distributed in the whole reactor.

To evaluate different options to minimize the short-circuiting, a case where feed stream was introduced from the bottom was considered. The outlet was modeled as overflow. For such a configuration (Figure 14c), the feed stream was introduced into the vessel against the pumping action of the impeller. The predicted exit age distribution is shown in Figure 13. It can be seen from Figure 13b that this combination of inlet and outlet locations further improved the mixing in the vessel. The predicted streak lines shown in Figure 14(c) indicate the interaction between inlet jet and impeller stream leading to better mixing. It may, however, be seen that the impeller-generated flow is not sufficient to disperse the injected feed homogeneously within the vessel. The particle streak lines are still not distributed all over the vessel. This suggests that possible increase in the impeller rotational speed might improve the extent of mixing. The flow in stirred vessel was then simulated for an impeller rotational speed of 720 rpm. The predicted exit age distribution for higher impeller rotational speed is shown in Figure 13. It can be seen from Figure 13 that the predicted exit age distribution is now closer to the ideal CSTR performance, as compared with the previous cases. The change in the location of inlet/outlet and increase in the impeller rotational speed was necessary to reduce the extent of by-passed fluid by more than half. Particle streak lines shown in Figure 14(d) also confirm that the incoming feed is distributed more or less in the whole vessel.

CFD models thus provide very useful information about the mixing behavior of continuously stirred vessels and may therefore be used to evaluate different alternative design configurations. The computational model and results discussed in this work will be useful for understanding the mixing process in continuous-flow stirred vessels.

CONCLUSIONS

The three-dimensional flow generated by an axial flow impeller, Mixel TT, was simulated using the MRF approach. The computational model was developed using a commercial CFD code, Fluent 5.3. The mean flow and turbulence characteristics were computed by solving the Reynolds averaged Navier–Stokes equations combined with the standard k–ε turbulence model.

The predicted results were compared with reported experimental results for the batch as well as the continuous-flow mode of operation. The predicted results show reasonably good agreement with the reported data for the batch mode of operation. Despite some discrepancies, the CFD model was able to capture the key features of the flow generated by the impeller. The computational model developed was used to study the characteristics of flow around the blades of the Mixel TT impeller. The simulated results show a single trailing vortex trailing behind the blades.

The model was then extended for simulating continuous-flow operation. The simulated flow field for the continuous operation also shows a reasonable agreement with the experimental data. The predicted results capture the key variations in flow characteristics in angular direction (feed and other r–z planes). The experimental and predicted flow fields indicate the possibility of short-circuiting and non-ideal flow behavior. The developed computational model was therefore further used to study the mixing process and the residence time distribution of the liquid in the continuous-flow operation of the stirred reactor. The predicted exit age distribution, the snapshots of tracer concentration and the streamlines of incoming feed explained the possible short-circuiting in the stirred reactor. Even for a high ratio of residence time to mixing time ($\tau/t_m = 9.6$), the possibility of short-circuiting was observed.

The predicted results indicate that the inlet and outlet locations may be the cause of short-circuiting for the present setup and operating conditions. The computational model was then used to devise the new inlet/outlet configuration, which will improve the mixing quality in the reactor. It was observed that the feed tube at the bottom of the reactor and overflow type outlet with impeller rotational speed of 720 rpm provides better mixing in the reactor for the present experimental setup and incoming liquid flow rate. The computational model shows promising results and seems to be a useful tool for designing and optimizing the performance of continuous stirred reactors.

NOMENCLATURE

C	impeller off-bottom clearance, m
D	impeller diameter, m
d_{in}	inlet pipe diameter, m
d_{out}	outlet pipe diameter, m
d_s	impeller shaft diameter, m
E_Θ	normalized RTD function
H	height of liquid from the bottom of the reactor, m
I	turbulent intensity
k	turbulent kinetic energy, $m^2 s^{-2}$
l	turbulent length scale, m
N	impeller rotational speed, rpm
N_Q	impeller pumping number
Q_l	volumetric flow rate, $m^3 s^{-1}$
r	radial distance from the axis of shaft, m
R	curvature of vessel bottom, m
R_{in}	hydraulic radius of feed pipe, m
T	vessel diameter, m
t_m	mixing time, s
U	mean axial velocity, $m s^{-1}$
V	mean radial velocity, $m s^{-1}$
V_l	liquid volume in reactor, m^3
W	mean tangential velocity, $m s^{-1}$
z	axial distance from the bottom of the reactor, m

Greek symbols

θ	angle from the leading edge of blade (angular coordinate)
τ	mean residence time, s
ρ	density, $kg m^{-3}$
ε	turbulent energy dissipation rate, $m^2 s^{-3}$
μ	viscosity, Pa s

REFERENCES

Aubin, J., Mavros, P., Bertrand, J., Fletcher, D. and Xuereb, C., 2001, Effect of axial agitator configuration (up-pumping, down-pumping, reverse rotation) on flow patterns generated in stirred vessels, *Chem Eng Res Des*, 79A(8): 845–856.

Baudou, C., Xuereb, C. and Bertrand, J., 1997, 3-D hydrodynamics generated in a stirred vessel by a multiple-propeller system, *Can J Chem Eng*, 75: 653–663.

Brucato, A., Ciofalo, M., Grisafi, F. and Micale, G., 1998, Numerical prediction of flow fields in baffled stirred vessels: a comparison of alternative modeling approaches, *Chem Eng Sci*, 53: 3653–3684.

Jenne, M. and Reuss, M., 1999, A critical assessment on the use of k-ε turbulence model for simulation of turbulent flow induced by a Rushton turbine in a baffled stirred tank reactor, *Chem Eng Sci*, 54: 3921–3941.

Marshall, E., Haidari, A. and Subbiah, S., 1996, *AIChE Annual Meeting*, Chicago, November.

Mavros, P., Xuereb, C. and Bertrand, J., 1996, Determination of 3-D flow fields in agitated vessels by laser Doppler velocimetry—effect of impeller type and liquid viscosity on liquid flow patterns, *Chem Eng Res Des*, 74A: 658–668.

Mavros, P., Naude, I., Xuereb, C. and Bertrand, J., 1997, Laser Doppler velocimetry in agitated vessels. Effect of continuous liquid stream on flow patterns, *Chem Eng Res Des*, 75A: 763–776.

Mavros, P., Barrue, H., Xureb, C., Foŕt, I. and Bertrand, J., 2000, Effect of axial-flow impeller and feed tube location on flow patterns in continuous flow stirred tank reactor, in *13th International Congress of Chemical and Process Engineering Conference, CHISA*.

Mavros, P., Xuereb, C., Foŕt, I. and Bertrand, J., 2002, Investigation by laser Doppler velocimetry of the effects of liquid flow rates and feed positions on the flow patterns induced in a stirred tank by an axial-flow impeller, *Chem Eng Sci*, 57: 3939–3952.

Ng, K., Fentiman, N.J., Lee, K.C. and Yianneskis, M., 1998, Assessment of sliding mesh CFD predictions and LDA measurements of the flow in a tank stirred by a Rushton impeller, *Chem Eng Res Des*, 76: 737–747.

Ranade, V.V., 2002, *Computational Flow Modeling for Chemical Reactor Engineering* (Academic Press, New York).

Ranade, V.V. and Tayaliya, Y., 2000, Computational study of transfer and dissipation of impeller power, in *ISHMT-15 Conference*, Pune, January 2000.

Ranade, V.V., Bourne, J.R. and Joshi, J.B., 1991, Fluid mechanics and mixing in agitated tanks, *Chem Eng Sci*, 46: 1883–1893.

Ranade, V.V. and van den Akker, H.E.A., 1994, Modelling of flow in gas–liquid stirred vessels, *Chem Eng Sci*, 49: 5175–5192.

Ranade, V.V., Perrard, M., Le Sauze, N., Xureb, C. and Bertrand, J., 2001, Trailing vortices of Rushton turbines, *Chem Eng Res Des*, 79A: 3.

Ranade, V.V., Krishnan, H. and Tayaliya, Y., 2002, CFD predictions of flow near impeller blades in baffled stirred vessels: assessment of computational snapshot approach, *Chem Eng Comm*, 189(7): 895–922.

Roe, P.L., 1985, Some contributions to the modelling of discontinuous flows, *Lecture Notes in Applied Mathematics*, Vol 22 (Springer), pp 163–193.

Rouston, M. and Pharamond, J.C., 1988, Agitation et mélange, *Tech Ing*, A.10: A5900.

Wechsler, K., Breuer, M. and Durst, F., 1999, Steady and unsteady computations of turbulent flows induced by a 4/45° pitched blade impeller, *J Fluids Eng*, 121: 318.

ACKNOWLEDGEMENTS

Part of this work was supported by Indo-French Center for the Promotion of Advanced Research (IFCPAR). One of the authors (A.R.K.) is grateful to CSIR for providing research fellowship. Thanks are due also to Dr J. Aubin for providing the CAD file with the geometrical details of the Mixel TT impeller.

The manuscript was received 11 April 2002 and accepted for publication after revision 18 February 2003.